https://doi.org/10.3311/PPCh.22867
Creative Commons Attribution

Periodica Polytechnica Chemical Engineering, 68(2), pp. 239–252, 2024

Biosorption of Cu(II) Ions by Water Hyacinth Leaf Powder: Process Performance, Kinetics, and Biosorption Isotherm

Ratnawati Ratnawati[1*], Aji Prasetyaningrum[1], Hargono Hargono[1], Muhammad Fahmi Zakaria[1]

[1] Department of Chemical Engineering, Faculty of Engineering, Universitas Diponegoro, Jl. Prof. Soedarto, Kampus Undip Tembalang, Semarang 50275, Indonesia
[*] Corresponding author, e-mail: ratnawati@che.undip.ac.id

Received: 24 June 2023, Accepted: 22 September 2023, Published online: 14 March 2024

Abstract

The water hyacinth leaf powder (WH) was used to adsorb Cu(II) from wastewater. The WH was modified through sulfuric acid (A-WH) and sodium hydroxide (B-WH) treatments. The biosorption was studied with various initial pH, initial Cu(II) concentrations, and biosorption time. The results show that the biosorption capacities of the biosorbents increase with the initial Cu(II) concentration. The optimum pH for the biosorption was 7.5, 7.0, and 7.5 for the WH, A-WH, and B-WH, respectively. The SEM images of the raw and treated WH revealed that alkali treatment could remove lignin more than the acid treatment, leaving more macropores in the B-WH than in the A-WH. The acid and alkali treatments to the WH leaf increase the biosorption capacity of the WH for Cu (II). The pseudo-second-order kinetic model can represent the dynamic behavior of the biosorption better than the pseudo-first-order model. The Langmuir model is better than the Freundlich model for describing the biosorption isotherm. The maximum biosorption capacities of the biosorbents predicted by the Langmuir model were 14.92 mg g^{-1}, 18.32 mg g^{-1}, and 23.27 mg g^{-1} for WH, A-WH, and B-WH, respectively.

Keywords

acid treatment, alkali treatment, biosorbent, biosorption, water hyacinth

1 Introduction

Water pollution caused by heavy metal waste from industrial activities is a global problem. Copper (Cu(II)) is one of the toxic contaminants in several industries, such as metal and electroplating, textile, leather, and mining industries [1–4]. Cu(II) is needed for human physiology in trace amounts, but it is harmful at a slightly higher concentration [5]. The World Health Organization stated that the maximum content of Cu(II) in drinking water is 2.0 mg L^{-1} [1]. Therefore, removing Cu(II) from wastewater is essential to reduce harmful effects.

The reduction of metal in wastewater has been the subject of numerous research using various techniques, including ion exchange, cementation, electrochemical approaches, photocatalysis, membrane filtering, and adsorption [6–12]. Among all methods, adsorption is simple with a low initial cost [1]. It is a potential method to remove heavy metals from wastewater, especially at low concentrations [13].

Various types of adsorbent, such as zeolite, activated carbon, nanosized hydroxyapatite, and nanocomposite, have been utilized to remove Cu(II) ions from aqueous solution [12, 14–16]. However, plant-based adsorbent, or biosorbent, attracted much attention due to its abundant availability, low cost, flexibility toward different contaminants, recyclability, and minimum sludge formation [17]. One of the advantages of the biosorbent is that it has a hydroxyl or carboxyl functional group, which has an affinity toward heavy metal ions [18].

Water hyacinth (*Eichornia crassipes*) has been used as a biosorbent for heavy metal removal [19–25]. Roots and stems are parts of water hyacinth widely used as a biosorbent [19–22]. Only a few studies reported the utilization of water hyacinth leaf as a biosorbent [23–25].

Water hyacinth, considered a weed, thrives in Rawa Pening Lake in Central Java, Indonesia. The villagers around the lake utilize dried water hyacinth stems for craft goods, such as furniture, handbags, and sandals. However, the leaves get little attention, most of which are composted. Therefore, it is necessary to explore the usage of water hyacinth leaves, one of which is a biosorbent for heavy metal removal from wastewater. Therefore, this work aimed to investigate the performance of water hyacinth leaf powder in adsorbing Cu(II) from an aqueous

Cite this article as: Ratnawati, R., Prasetyaningrum, A., Hargono, H., Zakaria M. F. "Biosorption of Cu(II) Ions by Water Hyacinth Leaf Powder: Process Performance, Kinetics, and Biosorption Isotherm", Periodica Polytechnica Chemical Engineering, 68(2), pp. 239–252, 2024. https://doi.org/10.3311/PPCh.22867

solution. The raw, along with the acid- and alkali-treated water hyacinth leaf powder, was utilized in this work. The effect of pretreatment of the water hyacinth leaf powder, pH, and the initial Cu(II) concentration on the metal removal was investigated. The Langmuir and Freundlich models were utilized to correlate and predict the adsorption isotherms. The kinetics and mechanism of the adsorption were investigated as well.

2 Materials and method

2.1 Materials

The materials used in this study were water hyacinth leaves, $CuNO_3 \cdot 2H_2O$, HCl, and NaOH. All the analytical grade chemicals were purchased from Merck (Sigma-Aldrich, Indonesia). The water hyacinth leaves were obtained from Rawa Pening Lake, Central Java, Indonesia. The water hyacinth leaves were washed, cut to ± 0.5 cm, air-dried, ground, and sieved to pass a 60-mesh sieve to obtain water hyacinth leaf powder (denoted as WH).

2.2 Delignification of WH

The WH was treated with acid and alkali using the method developed by Singh and Bishnoi with minor modifications [26]. The acid-treated WH (denoted as A-WH) was prepared by soaking the WH in a 2% (w/v) sulfuric acid solution to form a 10% (w/v) mixture. The mixture was heated in an autoclave at 100 °C for 40 minutes. The mixture was filtered using a Whatman 40 filter paper, and the residue was washed until it was neutral. The residue was dried in an oven at 75 ± 5 °C for 48 hours. The alkali-treated WH (denoted as B-WH) was prepared using the same method as the A-WH, except that the solution used was a 2% (w/v) sodium hydroxide solution. The prepared WH, A-WH, and B-WH biosorbents were stored in respective air-tight containers for the following experiments.

2.3 Characterization of WH biosorbents

Cellulose, hemicellulose, and lignin contents were determined using Chesson-Datta method [27]. The bisorbent's morphological features were obtained using the scanning electron microscope of model JSM-6360LV (JEOL Ltd., Tokyo, Japan). The morphological images of the samples were photographed at a magnification of 1000×. The existence of functional groups in WH, A-WH, and B-WH was analyzed using an FT-IR apparatus (Perkin Elmer PC 1600, Houston, TX, USA). The analysis was done by adding and mixing KBr salt with a ratio of 1:10. The samples were put in FT-IR cells. Then their characteristics were measured for the functional group within 4000–250 cm^{-1} of wavenumber.

2.4 Biosorption experiments

2.4.1 Experiments to determine the effect of pH

The dried WH, A-WH, and B-WH powder were soaked in deionized water for 6 h before it was used for biosorption experiments. In each run, 0.1 g of powder was used in 100 mL of Cu(II) solution with an initial concentration of 50 mg L^{-1} and initial pH of 5.0–8.0. The mixture was stirred at a speed of 200 rpm and a temparature of 28 ± 1 °C for 120 minutes. Then the mixture was filtered through a Whatman 40 filter paper to separate the biosorbent from the solution. Next, the solution was analyzed for Cu(II) concentration determination. The analysis was performed in triplicate. The following experiments used the optimum pH to investigate the biosorption isotherm and kinetics.

A preliminary experiment showed that the concentration of the solution was constant after the biosorption was conducted for 120 minutes. It means that the equilibrium was attained at 120 minutes. The biosorption capacity (q_e), defined as the amount of metal uptake at equilibrium per unit mass of biosorbent, and the removal efficiency are calculated using Eqs. (1) and (2), respectively [28]:

$$q_e = \frac{(C_0 - C_e)V}{m}, \tag{1}$$

$$\text{Removal efficiency} = \frac{C_0 - C_e}{m} \times 100\% . \tag{2}$$

The initial pH resulting in the highest q_e value is considered the optimum pH. It was used in the following experiments to investigate the biosorption isotherm and kinetics.

2.4.2 Experiment for biosorption kinetics

The experiment used WH, A-WH, and B-WH as the biosorbents, each with the optimum initial pH obtained in the previous experiment. The procedure was the same as in the experiment for determining the effect of pH (Section 2.4.1), except that the biosorbent used was 50 mg, and the biosorption time was varied (15, 30, 45, 60, 75, 90, 105, 120 minutes).

The mass of Cu(II) adsorbed per unit mass of biosorbent (q_t) at any time was calculated using Eq. (3) [28]:

$$q_t = \frac{(C_0 - C_t)V}{m}. \tag{3}$$

2.4.3 Experiments for biosorption isotherm

The experiment used three biosorbents, each with the optimum initial pH obtained in the previous experiment. The procedure was the same as in the experiment for

determining the effect of pH (Section 2.4.1), except that the biosorbent used was 50 mg, and the initial concentration of Cu(II) in the solution was varied (10–200 mg L^{-1}).

2.4.4 Determination of Cu(II) concentration

The Cu(II) concentration was determined using the atomic absorption spectroscopy apparatus (Shimadzu AA-670 spectrophotometer at 540 nm).

2.5 Biosorption kinetic models

2.5.1 Pseudo-first and second-order kinetic models

The pseudo-first-order (PFO) and pseudo-second-order (PSO) models were used to describe the kinetics of the biosorption of Cu(II) on the WH, A-WH, and B-WH. The linear forms of the PFO and PSO models are presented in Eqs. (4) and (5), respectively [28]:

$$\ln\left(q_e - q_t\right) = \ln q_e - k_f t, \tag{4}$$

$$\frac{t}{q_t} = \frac{t}{q_e} + \frac{1}{k_s q_e^2}. \tag{5}$$

2.5.2 Intraparticle diffusion model

Adsorption is a mass transport process that can be viewed as a diffusion. According to the intraparticle diffusion (IPD) model, the adsorption mechanism is through three steps, i.e., the external mass transfer, the intraparticle diffusion, and the final equilibrium step. In the first step, the adsorbate is transferred from the bulk solution to the external surface of the adsorbent through the boundary layer. In the second step, the adsorbate migrates from the external surface to the macropores inside the adsorbent. In the final step, the adsorbate moves slowly from the macropores to the micropores of the adsorbent [29].

Based on the IPD model, q_t is a linear function of $t^{0.5}$ according to Eq. (6):

$$q_t = k_i t^{0.5} + C. \tag{6}$$

where k_i and C can be obtained from the slope and intercept of q_t versus $t^{0.5}$ plot.

2.6 Biosorption isotherm models

2.6.1 Langmuir isotherm model

The Langmuir isotherm model is based on three assumptions:

1. monolayer adsorption (one molecule thickness);
2. the surface of the adsorbent has a finite number of identic sites for the adsorption;
3. there is no lateral interaction between the adsorbed molecules even they are on adjacent sites [30].

The Langmuir equation describes the amount of adsorbate adsorbed at equilibrium, (q_e), as presented in Eq. (7):

$$q_e = \frac{K_L q_m C_e}{1 + K_L C_e}. \tag{7}$$

Eq. (7) can be converted to a linear form as Eq. (8):

$$\frac{C_e}{q_e} = \left(\frac{1}{q_m}\right) C_e + \frac{1}{K_L q_m}. \tag{8}$$

A critical feature of the Langmuir adsorption isotherm is that it can predict the affinity of the adsorption through separation factor (R_L) defined in Eq. (9):

$$R_L = \frac{1}{1 + K_L C_0}. \tag{9}$$

Depending on the value of R_L, the adsorption can be categorized as unfavorable ($R_L > 1$), linear ($R_L = 1$), favorable ($0 < R_L < 1$), and irreversible ($R_L = 0 = 0$) [30].

2.6.2 Freundlich isotherm model

The Freundlich isotherm model assumes that the adsorption occurs on a heterogeneous surface. This model is represented by Eq. (10) [30]:

$$q_e = K_F C_e^{1/n}, \tag{10}$$

where K_F and $1/n$ are constants related to the adsorption capacity and intensity, respectively, which can be obtained from the plot of $\ln q_e$ against $\ln C_e$ according to Eq. (11):

$$\ln q_e = \ln K_F + \frac{1}{n} \ln C_e. \tag{11}$$

3 Results and discussion

3.1 Effect of pretreatment on the chemical composition of WH biosorbents

Table 1 shows the compositions of the raw and treated WH. The content of cellulose, hemicellulose, and lignin in the raw WH are 18.42%, 34.71%, and 5.22%, respectively.

Table 1 Effect of pretreatments on WH composition

Component	Composition (%)		
	WH	A-WH	B-WH
Cellulose	18.42	25.62	32.24
Hemicellulose	34.71	23.18	48.34
Lignin	5.22	4.68	2.27

After acid treatment, the cellulose content increases to 25.62%, while the hemicellulose and lignin contents decrease to 23.18% and 4.68%, respectively. Meanwhile, the alkali pretreatment causes the cellulose and hemicellulose content to increase to 32.24% and 48.34%, respectively, while lignin decreases to 2.27%. Singh and Bishnoi reported a similar result [26]. They reported that after dilute-acid (2% w/v HCl) pretreatment, the cellulose content increased from 19.2% to 24.2%, while the hemicellulose and lignin content decreased from 40.0% to 27.5% and from 4.8 to 3.6%, respectively. They also revealed that dilute alkali (2% w/v NaOH) pretreatment caused the percentage of cellulose and hemicellulose increased from 19.2% to 32.4% and from 40.0% to 55%, respectively, while lignin decreased from 4.8% to 2.1%.

During dilute acid and alkali pretreatment, the acid and alkali disrupt the cell wall by attacking the ferulic acid bridge connecting hemicellulose and lignin through ester and ether bonds [31]. It is shown in Fig. 1 that the ester linkage connecting hemicellulose and ferulic acid is susceptible to alkali attack. In contrast, the ether linkage connecting lignin and ferulic acid is susceptible to acid attack.

In the dilute acid pretreatment, the acid further attacks the glycosidic bond of hemicellulose, leading to a hydrolysis reaction to smaller molecules soluble in water [32]. It could be the reason why the content of hemicellulose decreases during dilute acid pretreatment. Lignin is also depolymerized due to the presence of acid. The cleavage of β-O-4 structures results in the formation of free phenolic moieties and Hibbert ketones [33], which will quickly condensate and precipitate in acidic environments [32], so the lignin content decreases but not as much as hemicellulose. Unlike hemicellulose and lignin, cellulose is not affected much by dilute acid at 100 °C. Therefore, the amount of cellulose could decrease, but not as much as hemicellulose and lignin. As a result, the percentage of cellulose increases.

Dilute alkali treatment increases cellulose and hemicellulose contents to 32.24% and 48.34%, respectively, while lignin content decreases to 2.27%. Singh and Bishnoi [26] found the same trend. Due to NaOH dissociation, the hydroxide ion attacks the ester bond between the ferulic acid and hemicellulose fractions, opening up the "lignin wall" of the lignocellulose allowing lignin components to be solubilized and making both cellulose and hemicellulose accessible to the alkali solution [34, 35]. Therefore, alkali pretreatment can remove lignin in plant tissues effectively, resulting in high delignification [36], as it is presented in Table 1 that the percentage of lignin decreases from 5.22% to 2.27%. As the hemicellulose and cellulose are accessible to the alkali solution, the hemicellulose fraction may be degraded. Meanwhile, at the experimental condition of this work (100 °C and 2 g NaOH/100 mL solution), the glycosidic (1 → 4)-linkages between the β-D-glucopyranose units in cellulose are stable, so the structural change of cellulose is insignificant. Alkali solutions may cause swelling, de-crystallization, and cellulose depolymerization, increasing the lignocellulosic material's internal area and porosity [35].

3.2 Effect of pretreatment on the morphology of WH biosorbents

SEM micrographs of the WH, A-WH, and B-WH are shown in Fig. 2 (a)–(c), respectively. It is seen in Fig. 2 (a) that there are only a few small pores (with a diameter < 10 μm) on the WH surface, as marked with small red circles. After acid treatment, the surface of A-WH becomes rougher, and some larger pores (with a diameter < 26 μm) are observed, as depicted in Fig. 2 (b) and marked with red circles and an ellipse. These pores result from the disruption of the lignocellulosic cell wall by the acid [32], leaving more and larger pores, as explained earlier. Alkali treatment causes more lignin solubilization and attack of hemicellulose by the alkali [35], leading to even more and larger pores (with diameters up to 76 μm) forming on the B-WH surface, as shown in Fig. 2 (c). All pores observed in Fig. 2 (a)–(c) are categorized as macropores (diameter > 200–300 nm) [37].

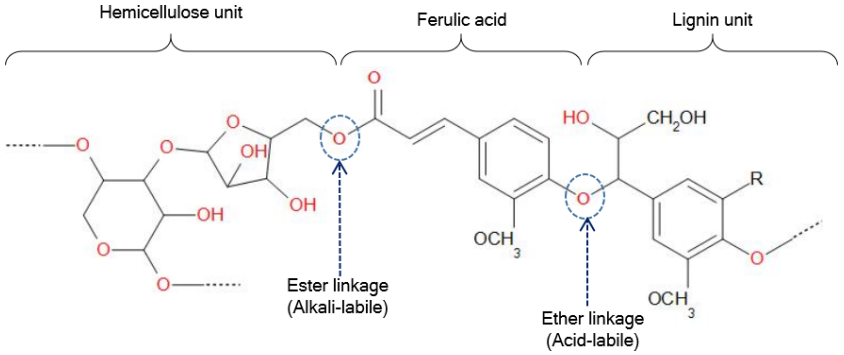

Fig. 1 The cleavage sites of lignocellulosic complexes during pretreatments using acid and alkali (adapted from Oriez et al. [31])

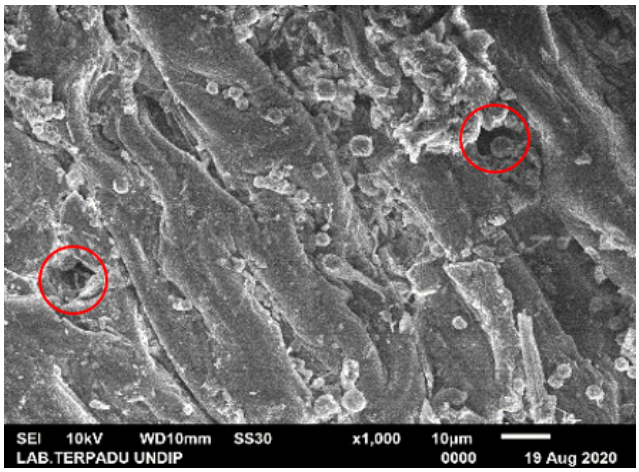

(a)

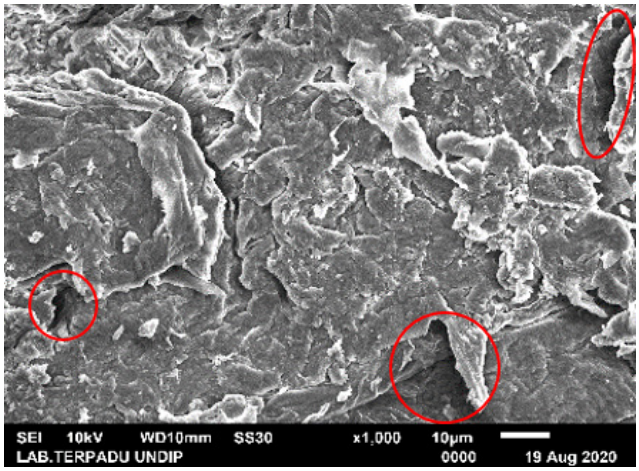

(b)

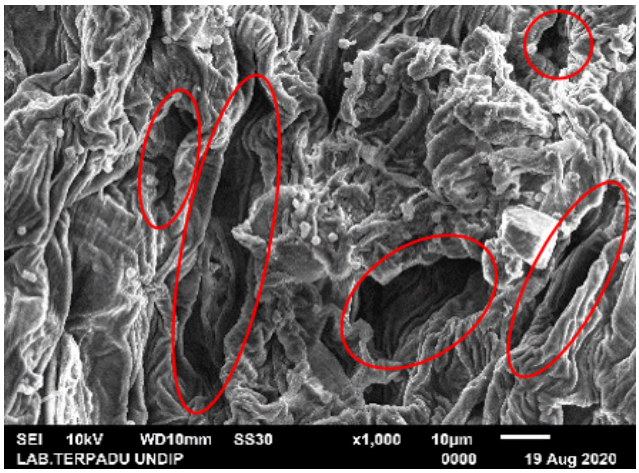

(c)

Fig. 2 (a) SEM images of WH, (b) A-WH, (c) and B-WH; red markings: observable macropores

3.3 Characterization of WH biosorbents

Fig. 3 shows the absorbance spectra of WH, A-WH, and B-WH, which can be distinguished into two regions,

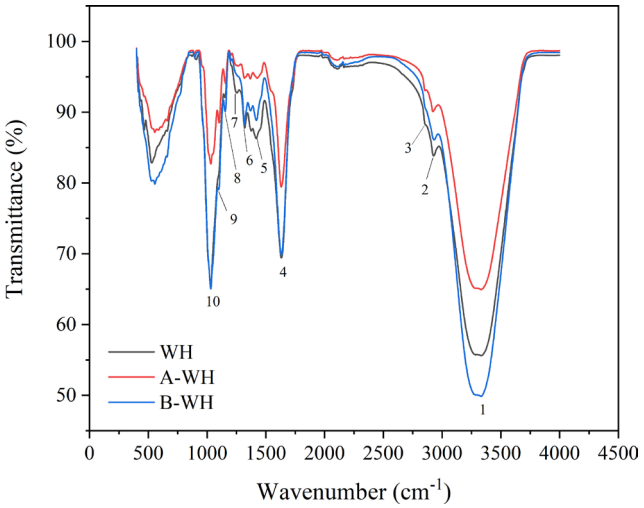

Fig. 3 FTIR spectra of WH, A-WH, and B-WH

i.e., 3800–2800 cm^{-1} and 1800–800 cm^{-1}. The peak numbers and the assigned functional groups are listed in Table 2. The first region consists of three peaks (1, 2, and 3) that are assigned to hydrogen-bonded OH intramolecular and intermolecular stretching, symmetric and asymmetric C-H stretching, respectively. These functional groups are present in cellulose, hemicellulose, and lignin. The second group is the fingerprints region [38] where many peaks are assigned to cellulose (peaks 6 and 8), lignin (peaks 5 and 7), hemicellulose and lignin (peak 4), cellulose and hemicellulose (peak 9), as well as cellulose and lignin (peak 10).

Peaks 6 and 8 are assigned to CH_2 wagging and C-O-C asymmetric stretching, respectively, present in cellulose [38]. Both peaks are slightly more prominent in A-WH and B-WH than in WH, as depicted in Fig. 3. It is in line with the chemical analysis of the biomass presented in Table 1, in which the cellulose content in A-WH and B-WH are higher than in WH. Peaks 5 and 7 correspond to C=O stretching in aromatic skeletal vibration with C-H deformation and syringyl ring and C-O stretch, respectively, in lignin molecular structure [38, 39]. Peak 5 disappears in A-WH, but it is still observable in B-WH. Meanwhile, peak 7 completely recedes in A-WH and B-WH. It means there is a decrease in lignin content in A-WH and B-WH, as confirmed by the analysis result in Table 1.

Peak 4 at a wavenumber of 1629 cm^{-1} is assigned to C=O stretching in carboxylic group in hemicellulose and lignin [40] and H-O-H bending of water molecules adsorbed on the biomass [41]. It is shown in Fig. 3 that this wavenumber is absorbed more by the WH than A-WH. It is in accordance with the chemical analysis that WH contains less hemicellulose than A-WH, as presented in Table 1.

Table 2 Assignment of peaks in FTIR spectra of water hyacinth leaf powder

Peak number	Wavenumber (cm^{-1})	Functional group	Component	Ref.
1	3318	Hydrogen-bonded OH intramolecular and intermolecular stretching	Cellulose, hemicellulose, lignin	[38]
2	2910	Symmetric methyl and methylene stretching	Cellulose, hemicellulose, lignin	[38]
3	2840	Asymmetric methyl and methylene stretching	Cellulose, hemicellulose, lignin	[38]
4	1629	C=O stretching in carboxylic group	Hemicellulose, lignin	[40]
		H-O-H bending of absorbed water molecules	Water molecules absorbed on the sample	[41]
5	1415	C=O stretching in aromatic skeletal vibration with C-H deformation	Lignin	[38, 39]
6	1334	CH_2 wagging	Cellulose	[38]
7	1244	Syringyl ring and C-O stretch	Lignin	[39]
8	1149	C-O-C asymmetric stretching	Cellulose	[38]
9	1100	C-O-C stretching and aromatic C-H in-plane deformation	Cellulose, hemicellulose	[38]
10	1038	C-O stretching, aromatic C-H in-plane deformation	Cellulose, lignin	[38]

Peak 9 (wavenumber 1100 cm^{-1}) represents C-O-C stretching and aromatic C-H in-plane deformation in cellulose and hemicellulose [38]. This peak is more observable in A-WH and B-WH than in WH. It conforms to the chemical analysis presented in Table 1, showing that cellulose and hemicellulose content is higher in A-WH and B-WH than in WH. Peak 10 at a wavenumber of 1038 cm^{-1} is assigned to the stretching vibration of C-O and aromatic C-H in-plane deformation of cellulose and lignin [38].

3.4 Effect pH on the biosorption of Cu(II) ions

Fig. 4 shows the effect of pH on the biosorption of Cu(II) ions by raw and treated WH. The biosorption capacity of the three biosorbents increases as pH increases and reaches optimum values at pH 7.5, 7.0, and 7.5 for WH, A-WH, and B-WH, respectively, with the amount of Cu(II) ion adsorbed as much as 12.34, 16.15, and 23.08 mg g^{-1}, respectively. Uddin et al. [42] used acid-treated water hyacinth to adsorb methylene blue from a solution with various pH. They reported that the biosorption capacity of the biosorbent reached the optimum value at a pH of 6.934. Guyo and Moyo [43] adsorbed Pb(II) from a solution using cowpea pod-based adsorbent at pH 2 to 8. They found that the biosorption capacity reached the optimum value at a pH of 6. The poor adsorption of ionic metal in acidic conditions is partly caused by protons (H^+). At low pH, the concentration of proton is high, possibly occupying the binding sites on the surface of the adsorbent, reducing the available sites for the metal ions. When the pH increases, the proton concentration decreases, leaving more sites on the adsorbent surface for the metal ion [44].

It is seen in Fig. 4 that the biosorption capacities of both the A-WH and B-WH are better than that of the WH,

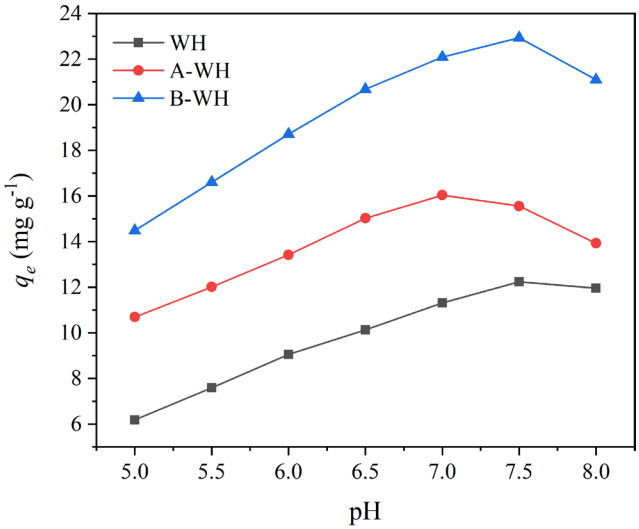

Fig. 4 The effect of pH on the biosorption capacity of WH, A-WB, and B-WH for Cu(II) ions removal

in which the B-WH has the highest biosorption capacity. It means that both acid and alkali treatments can improve the biosorption capacity of the WH biosorbent. It can be related to the effect of acid and alkali on the structure of the WH leaves, as explained earlier. The acid treatment causes the formation of larger macropores, thus increasing the surface area for biosorption. Meanwhile, alkali treatments form more pores with larger diameters, as exhibited by the SEM micrograph in Fig. 2 (c). Consequently, the surface area of the B-WH is larger than those of the WH and A-WH.

3.5 Effect of initial concentration of Cu(II) ions

The biosorption capacity of the three biosorbents at various initial Cu(II) concentrations is shown in Fig. 5 (a). The biosorbent having the highest biosorption capacity is B-WH, followed by A-WH and WH. The biosorption capacities

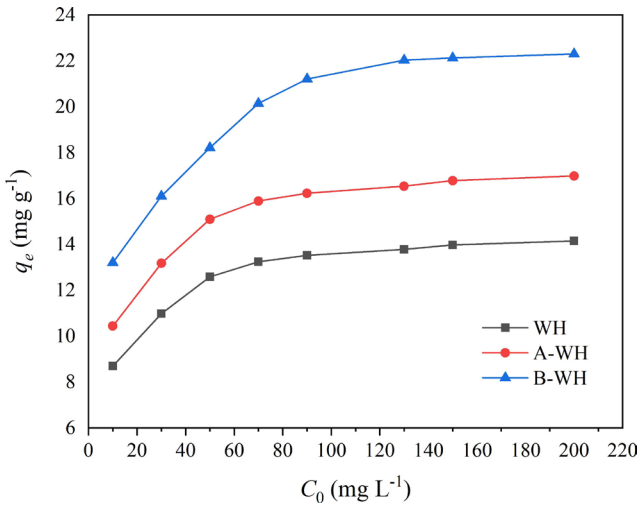

(a)

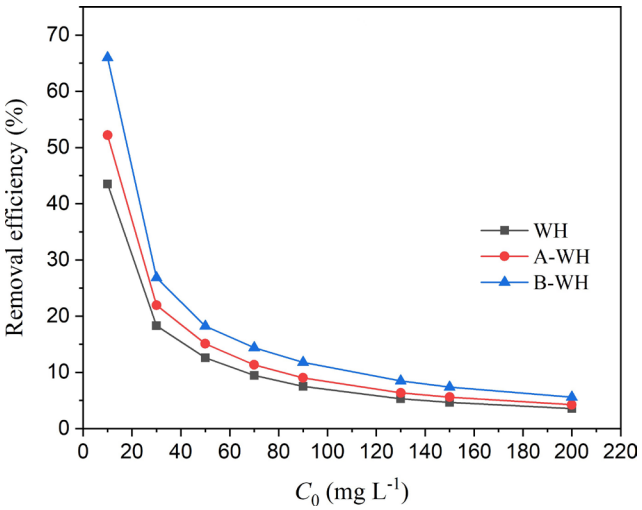

(b)

Fig. 5 Effect of initial concentration of Cu(II) ions on biosorption capacity (a) and removal efficiency (b) of WH, A-WH, and B-WH

of B-WH, A-WH, and WH for the initial Cu(II) concentration of 10 mg L^{-1} are 13.20, 10.44, and 8.70 mg g^{-1}, respectively. The biosorbent capacities of all biosorbents increase as the initial Cu(II) concentration increases. However, the biosorption capacities are almost constant at an initial concentration above 70 mg L^{-1}. At an initial Cu(II) concentration of 200 mg L^{-1}, the biosorption capacities for the B-WH, A-WH, and WH reach 22.30, 16.98, and 14.15 mg g^{-1}, respectively. Many researchers reported similar results [45, 46].

The biosorbent's performance can be evaluated in terms of removal efficiency, as shown in Fig. 5 (b). It is seen in the figure that the B-WH results in the highest removal efficiency, followed by A-WH and WH. The removal efficiency of B-WH, A-WH, and WH drop sharply from 66.00% to 26.83%, 52.20% to 21.96%, and 43.50% to 18.30%, respectively, as the initial Cu(II) concentration increases from 10 to 30 mg L^{-1}. It continues to drop as the initial Cu(II) concentration increases but is not as sharp as the initial Cu(II) concentration increases from 10 to 30 mg L^{-1}. It eventually reaches 5.57%, 4.25%, and 3.54% for B-WH, A-WH, and WH, respectively, when the initial Cu(II) concentration is 200 mg L^{-1}. Other researchers reported similar results [45, 46].

The effect of the initial concentration of Cu(II) on the biosorption capacity could be related to the availability of the active sites on the surface of the biosorbent. The initial concentration of the solute renders the driving force for the mass transfer of the solute from the bulk solution to the surface of the biosorbent [47–49]. A kinetic study of the biosorption in this work shows that the biosorption is faster in higher initial Cu(II) concentrations. The interaction between Cu(II) and the biosorbent can occur more intensely in higher Cu(II) concentrations. Therefore, a higher initial Cu(II) concentration leads to higher biosorption [46].

Based on Fig. 5 (b), the removal efficiency is lower for higher initial Cu(II) concentrations. It is because the number of Cu(II) ions is much higher than the number of the active site on the biosorbent, leaving more Cu(II) ions unadsorbed in the bulk solution [49, 50]. As a result, the removal efficiency is lower for biosorption with a higher initial Cu(II) concentration.

3.6 Biosorption kinetics

Fig. 6 depicts the effect of time on Cu(II) biosorption on WH. It is shown that at the same time, the amount of

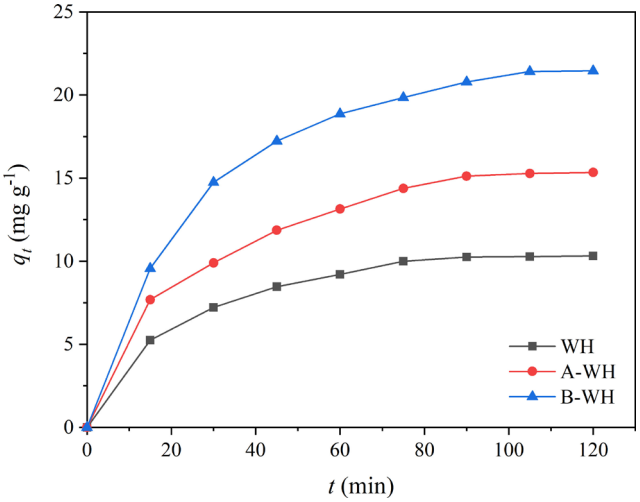

Fig. 6 Effect of time on the biosorption of Cu(II) ions on WH, A-WH, and B-WH

Cu(II) adsorbed (q_t) by the B-WH is higher than that by the A-WH and WH. The q_t of all biosorbents increases with time. The results show that q_t increases sharply in the first 30 minutes, but after that, the biosorption proceeds more slowly, and after 105 minutes, it becomes nearly constant.

Biosorption is a mass transfer process with a concentration gradient as the driving force [50]. The concentration gradient is the highest at the beginning of the process, so the biosorption proceeds fast. As the active site on the surface of the biosorbent is occupied by the adsorbate, the driving force becomes lower, and hence the biosorption process becomes slower.

3.6.1 The PFO and PSO kinetics model

For the PFO kinetic model, the experimental data was plotted as ln ($q_e - q_t$) versus t, as depicted in Fig. 7. Then, the data were fitted to the model (Eq. (4)) to obtain the model's parameters. The q_e was obtained from the intercept, while k_f was calculated from the slope of the linear plot. The parameters of the PFO model for the three biosorbents, along with the coefficients of determination (R^2), are presented in Table 3. It is shown in the table that the experimental data for the three biosorbents are fitted well to the model as their R^2 are 0.9819, 0.9847, and 0.9878 for the WH, A-WH, and B-WH, respectively. In addition, the PFO rate constants of the WH, A-WH, and B-WH are 0.040, 0.0343, and 0.0349 min^{-1}, respectively, while the biosorption capacities (q_e) are 10.42, 15.64, and 21.81 mg g^{-1}, respectively.

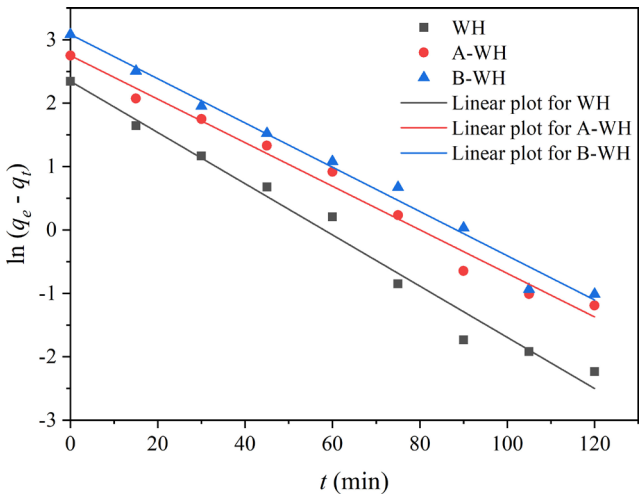

Fig. 7 Linear plot of the pseudo-first-order kinetic model of the biosorption of Cu(II) ions on WH, A-WH, and B-WH

The linear PSO kinetic model is depicted in Fig. 8. By fitting the data to Eq. (5), q_e and k_s can be obtained from the slope and intercept of the plot, respectively. The constants are presented in Table 3. The coefficients of determination (R^2) of the WH, A-WH, and B-WH models are 0.9977, 0.9965, and 0.9987, respectively. The PSO rate constants of the WH, A-WH, and B-WH are 4.172 × 10^{-3}, 2.220 × 10^{-3}, and 1.605 × 10^{-3} g mg^{-1} min^{-1}, respectively, while the biosorption capacities are 12.225, 18.692, and 26.110 mg g^{-1}, respectively.

In comparison to the PFO model, the PSO model produces greater R^2 and lower RSME values for all biosorbents. The higher value of R^2 and smaller RMSE correspond to a higher model fit [51]. Other researchers reported that the PSO fitted well with the experimental data [51–53].

3.6.2 Intraparticle diffusion model

The kinetic study using the PFO and PSO cannot explain the diffusion mechanism. Therefore, an analysis of the biosorption kinetics using the IPD model is necessary. The linearized IPD model is depicted in Fig. 9 as a plot of $t^{0.5}$ versus q_t. It is seen in the figure that a single straight line cannot approximate each set of data of the three biosorbents. Two or three linear plots of q_t versus $t^{0.5}$ can be considered in such a case. Each linear line represents a step in the biosorption mechanism. The first step, represented by the black straight line starting from the origin, is the external diffusion of the adsorbate from the bulk solution to the surface of the biosorbent through the stationary film or the boundary layer. The second step, represented by the red straight line, is intraparticle diffusion. The third step, represented by the blue straight line, is the final equilibrium step [29].

Two straight lines can approximate the data for the WH, while each A-WH and B-WH is represented by three straight lines, as shown in Fig. 9. The regression results are presented in Table 4. The biosorption rate constants

Table 3 Parameters of the PFO and PSO kinetics models for the biosorption of Cu(II) ions on raw and treated water hyacinth leaf powder

Biosorbent	PFO model				PSO model				Ref.
	q_e	k_f	R^2	RSME	q_e	k_s	R^2	RSME	
WH	10.4270	0.0404	0.9819	0.2225	12.2249	0.00417	0.9977	0.1549	This work
	2.3000	0.0450	0.9740	–	2.3900	0.1800	0.9820	–	[53]
A-WH	15.6441	0.0343	0.9847	0.5219	18.6916	0.00222	0.9965	0.3100	This work
B-WH	21.8135	0.0349	0.9878	0.3423	26.1097	0.00160	0.9987	0.2410	This work

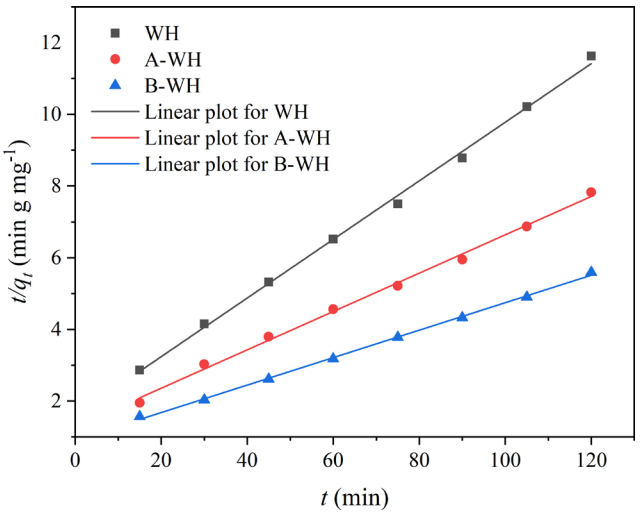

Fig. 8 Linear plot of the pseudo-second-order kinetic model of the biosorption of Cu(II) ions on WH, A-WH, and B-WH

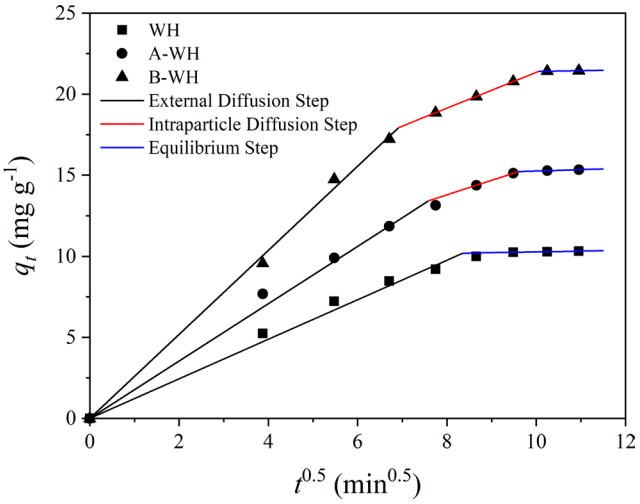

Fig. 9 Linear plot of the intraparticle diffusion kinetic model of the biosorption of Cu(II) ions on WH, A-WH, and B-WH

Table 4 Parameters of the IPD model for the biosorption of Cu(II) ions on WH, A-WH, and B-WH

Stage	Parameter	WH	A-WH	B-WH
	C	0	0	0
1	k_{i1}	1.2198	1.7687	2.5933
	R^2	0.9970	0.9978	0.9991
	C		6.6269	10.3140
2	k_{i2}		0.8953	1.1025
	R^2		1.0000	0.9999
	C	9.7965	14.4110	20.9860
3	k_{i3}	0.0476	0.0848	0.0424
	R^2	0.9894	1.0000	1.0000

for the first, second, and third steps are k_{i1}, k_{i2} and k_{i3}, respectively. It is seen in the table that for each biosorbent, $k_{i1} > k_{i2} > k_{i3}$. Sun and Yang [54] reported a similar trend for the biosorption of dyes from aqueous solution on modified peat-resin particles.

The data of the WH from t = 0 to 75 min ($t^{0.5}$ = 0 to 8.66 min$^{0.5}$) can be approximated by a straight line starting from the origin with k_{i1} = 1.2198 mg g^{-1} min$^{-0.5}$ and R^2 = 0.9970 as presented in Table 4. This line describes the external diffusion process in which the adsorbate moves from the bulk solution to the external surface of the biosorbent through the boundary layer. According to Fig. 9, this line is followed by a flat line representing the final equilibrium step with k_{i3} = 0.0476 mg g^{-1} min$^{-0.5}$ and R^2 = 0.9894. It could be related to the intact structure of the lignocellulosic wall of the raw WH, with only a few small-sized macropores observed, as exhibited by the SEM micrograph in Fig. 2 (a). A similar phenomenon was reported by Dizge et al. [55]. For the adsorption of reactive dyes from aqueous solution onto fly ash, the plot of q_t versus $t^{0.5}$ could be represented by two straight lines.

The biosorption of Cu(II) ions on A-WH can be represented by three straight lines, as shown in Fig. 9, which reflects the biosorption mechanism. The first step, representing the external diffusion, starts from the origin to t = 60 min ($t^{0.5}$ = 7.75 min$^{0.5}$). The straight-line regression results in k_{i1} = 1.7687 mg g^{-1} min$^{-0.5}$ and R^2 = 0.9978, as shown in Table 4. The second line, starting from t = 75 to 90 min ($t^{0.5}$ = 8.66 to 9.89 min$^{0.5}$), represents the intraparticle diffusion through macropores with k_{i2} = 0.8953 mg g^{-1} min$^{-0.5}$ and R^2 = 1.0. The value of $k_{i2} < k_{i1}$ means that the intraparticle diffusion through macropores is much slower than the external diffusion. The intraparticle diffusion is possible because the acid treatment disrupts the lignocellulosic wall of the WH, leaving several medium-sized macropores, as observed in Fig. 2 (b). However, this step occurs only briefly (from t = 75 to 90 min). The intraparticle diffusion through micropores or the equilibrium step starts after t = 105 min ($t^{0.5}$ = 10.95 min$^{0.5}$). The regression of this step results in k_{i3} = 0.0424 mg g^{-1} min$^{-0.5}$ and R^2 = 1.0. Sun and Yang [54] reported that the adsorption of dyes from aqueous solution onto modified peat-resin particles could be represented by three straight lines.

The B-WH shows the same trend as the A-WH in that the biosorption occurs in three steps. The external diffusion step can be approximated by a straight line starting from the origin to t = 45 min ($t^{0.5}$ = 6.71 min$^{0.5}$) with k_{i1} = 2.5933 mg g^{-1} min$^{-0.5}$ and R^2 = 0.9991. The intraparticle diffusion step occurs faster (k_{i2} = 10.3140 mg g^{-1} min$^{-0.5}$) and longer (from t = 60 to 90 min) than in the A-WH. It could be related to the existence of more large-sized macropores,

exhibited in Fig. 2 (c), as the results of alkali treatment to the WH. The final step of the biosorption occurs afterward with k_{i3} = 0.0848 mg g^{-1} min$^{-0.5}$ and R^2 = 1.0.

Based on the explanation above, it is proposed that the mechanism of Cu(II) biosorption on the WH is through two steps, i.e., external diffusion and intraparticle equilibrium diffusion. However, A-WH and B-WH have more and larger macropores, so the biosorption mechanism is proposed to consist of three steps, i.e., external diffusion, intraparticle diffusion through macropores, and intraparticle diffusion through micropores or the equilibrium step.

3.7 Biosorption isotherm

Fig. 10 shows the linear regression of the Langmuir isotherm model for Cu(II) biosorption onto WH, A-WH, and B-WH, i.e., a plot of C_e/q_e versus C_e. The constants q_m and K_L are obtained from the line slope and intercept, respectively, and are presented in Table 5. The coefficient of determinations for the WH, A-WH, and B-WH are > 0.99, indicating the Langmuir model's suitability to describe the biosorption of Cu(II) onto the raw and treated WH. The highest biosorption capacity is that of the B-WH (23.202 mg g^{-1}), followed by A-WH (17.413 mg g^{-1}) and WH (14.556 mg g^{-1}).

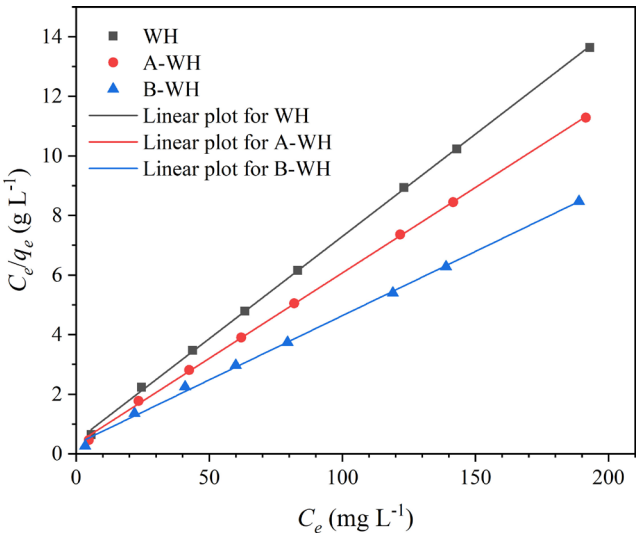

Fig. 10 Linear plot of Langmuir isotherm for the biosorption of Cu(II) ions on WH, A-WH, and B-WH at 30 °C

Adsorption is a surface phenomenon. The adsorption capacity of an adsorbent is related to the specific surface area. Different preparation methods of the adsorbents result in different specific surface areas, pore structure, and distribution, and hence different adsorption effects [56]. As is seen in Fig. 2, the surface of the WH is smooth, with only very few small-sized macropores. The A-WH is rougher with more medium-sized macropores. At the same time, B-WH is rougher with many large-sized macropores, so it is possible that the total external and internal surface area of the B-WH > A-WH > WH. It is seen in the Table 5 that the biosorption capacity of the WH, A-WH, and B-WH of this work are higher than that of the WH-based biochar [53], *Lepiota hystrix* biomass [57], and peanut hull [13]. Only *Aspergillus niger* was reported to have a higher value of q_m. However, it has a much lower K_L [58].

The affinity constants (K_L) of the three biosorbents are almost the same, i.e., 0.1603, 0.1715, and 0.1315 L mg^{-1} for the WH, A-WH, and B-WH, respectively. This constant is used to calculate the separation factor (R_L) of the adsorption process using Eq. (9). With an initial concentration of the adsorbate in the solution of 10 to 200 mg L^{-1}, the separation factors for the WH, A-WH, and B-WH are from 0.0305 to 0.3842, from 0.0284 to 0.3683, and from 0.0366 to 0.4320, respectively. All R_L are between 0 and 1, meaning the adsorption process using the three biosorbents is favorable [30]. The affinity constants of the three biosorbents in this work are higher than those of the other biosorbents reported by other researchers [13, 58].

Table 5 The Langmuir constants for the biosorption of Cu(II) ions on different biosorbents

Biosorbent	Langmuir model			Freundlich model			Ref.
	K_L (L mg^{-1})	q_m (mg g^{-1})	R^2	K_F (mg$^{1-1/n}$ L$^{1/n}$ g^{-1})	q_m (mg g^{-1})	R^2	
WH	0.1603	14.556	0.9996	6.828	6.609	0.9702	This work
A-WH	0.1715	17.422	0.9996	8.457	6.912	0.9735	This work
B-WH	0.1315	23.202	0.9983	10.745	6.743	0.9748	This work
WH-based biochar	6.830	2.06	0.9920	2.58	1.99	0.978	[53]
Lepiota hystrix biomass	–	8.58	0.9890	17.51	3.3158	0.969	[57]
Peanut hull (25 °C)	0.0822	13.587	0.9940	10.4590	27.473	0.5505	[13]
Peanut hull (35 °C)	0.0960	14.006	0.9980	10.6460	24.876	0.7368	[13]
Aspergillus niger	0.0150	33.23	0.9390	1.95	2.83	–	[58]

Fig. 11 shows the linear regression for the Freundlich isotherm model for Cu(II) biosorption using WH, A-WH, and B-WH as the biosorbent. The lines were obtained by plotting ln q_e against ln C_e. The regression results, including K_F, n, and R^2, are listed in Table 5. The Freundlich constants K_F are 6.828, 8.457, and 10.745 for the WH, A-WH, and B-WH, respectively, while the values of n are 6.609, 6.912, and 6.743, respectively, as listed in Table 5. The values of n for all three biosorbents are between 1 and 10, which means that the WH, A-WH, and B-WH have good potential as biosorbents [55]. The model's coefficient of determination (R^2) for the WH, A-WH, and B-WH are 0.9702, 0.9735, and 0.9748, respectively. These values are high enough for a regression. However, these values are less than those for the Langmuir model. It means that the biosorption of Cu(II) onto raw and treated WH is more suitable to be represented by the Langmuir isotherm model.

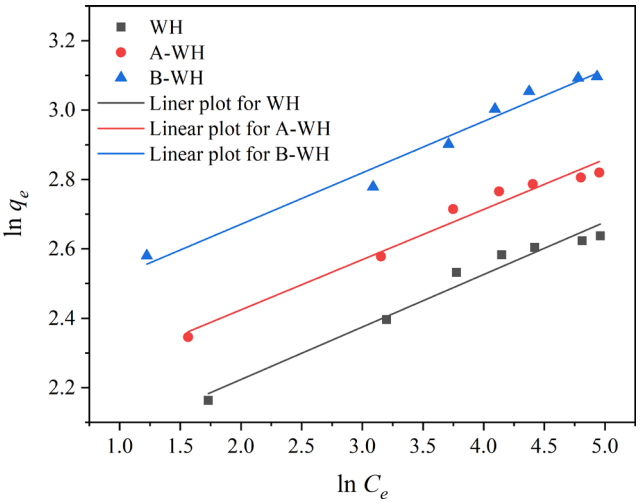

Fig. 11 Linear plot of Freundlich isotherm for the biosorption of Cu(II) ions on WH, A-WH, and B-WH at 30 °C

4 Conclusions

This work shows that water hyacinth can be used as a biosorbent to remove Cu(II) ions from aqueous solutions after it is chemically modified using acid and alkali. It has been confirmed that alkali treatment can remove lignin more than acid treatment. The amount of Cu(II) ions adsorbed by WH, A-WH, and B-WH reaches a maximum when the initial pH of the solution is 7.5, 7.0, and 7.5, respectively. The PSO kinetic model well represents the kinetics of the adsorption. Analysis of the IPD model reveals that the mechanism of biosorption of Cu(II) onto WH is through external diffusion (for all three biosorbents), followed by macropore diffusion (for A-WH and B-WH) and micropore diffusion in the final equilibrium step (for all three biosorbents). The biosorption capacity of WH leaf increases after acid and alkali treatment due to more medium and large-sized macropores formed. The equilibrium data follow the Langmuir isotherm equation, confirming the monolayer sorption of Cu(II) by WH, A-WH, and B-WH with a monolayer sorption capacity of 14.556, 17.422, and 23.202 mg g^{-1}, respectively.

Acknowledgments

The authors would like to thank Universitas Diponegoro for its laboratory facility.

Nomenclature

C: IPD model constant (mg g^{-1});
C_0: initial concentration of Cu(II) (mg L^{-1});
C_t: concentration of Cu(II) at t minutes (mg L^{-1});
C_e: concentration of Cu(II) at equilibrium (mg L^{-1});
k_f: PFO rate constant (min^{-1});
k_s: PSO rate constant (g mg^{-1} min^{-1});
k_i: IPD rate constant (mg g^{-1} min$^{-0.5}$);
K_F: constant of Freundlich model (mg$^{1-1/n}$ L$^{1/n}$ g^{-1});
K_L: affinity constant of Langmuir model (L mg^{-1});
q_e: adsorption capacity (mg g^{-1});
m: mass of biosobent (g);
n: constant of Freundlich model;
q_m: maximum mass of adsorbate adsorbed (mg g^{-1});
q_t: mass of Cu(II) adsorbed per unit mass of biosorbent (mg g^{-1});
R_L: separation factor;
t: time (min);
V: volume of Cu(II) solution (L).

References

[1] Al-Saydeh, S. A., El-Naas, M. H., Zaidi, S. J. "Copper removal from industrial wastewater: A comprehensive review", Journal of Industrial and Engineering Chemistry, 2017, 56, pp. 35–44, 2017. https://doi.org/10.1016/j.jiec.2017.07.026

[2] Türksoy, R., Terzioğlu, G., Yalçin, I. E., Terzioğlu, O. Y., Demir, G. "Removal of heavy metals from textile industry wastewater", Frontiers in Life Sciences and Related Technologies, 2(2), pp. 44–50, 2010. https://doi.org/10.51753/flsrt.958165

[3] Habila, B., Chidiebere, E. E., Hassana, D., Joseph, I. O., Bwankhot, S. T. "Determination of Heavy Metals in Tannery Wastes", International Journal of Agricultural and Biosystems Engineering, 3(3), pp. 78–81, 2018.

[4] Milićević, S., Vlahović, M., Kragović, M., Martinović, S., Milošević, V., Jonanović, I., Stojmenović, M. "Removal of Copper from Mining Wastewater Using Natural Raw Material–Comparative Study between the Synthetic and Natural Wastewater Samples", Minerals, 10(9), 753, 2020. https://doi.org/10.3390/min10090753

[5] Priyadarshanee, M., Das, S. "Biosorption and removal of toxic heavy metals by metal tolerating bacteria for bioremediation of metal contamination: A comprehensive review", Journal of Environmental Chemical Engineering, 9(1), 104686, 2021. https://doi.org/10.1016/j.jece.2020.104686

[6] Bashir, A., Malik, L. A., Ahad, S., Manzoor, T., Bhat, M. A., Dar, G. N., Pandith, A. H. "Removal of heavy metal ions from aqueous system by ion-exchange and biosorption methods", Environmental Chemistry Letters, 17(2), pp. 729–754, 2019. https://doi.org/10.1007/s10311-018-00828-y

[7] Nassef, E. "Removal of copper from wastewater by cementation from simulated leach liquors", Journal of Chemical Engineering & Process Technology, 6(1), 214, 2015. https://doi.org/10.4172/2157-7048.1000214

[8] Pedersen, K. B., Ottosen, L. M., Jensen, P. E., Lejon, T. "Comparison of 2-compartment, 3-compartment and stack designs for electrodialytic removal of heavy metals from harbour sediments", Electrochimica Acta, 181, pp. 48–57, 2015. https://doi.org/10.1016/j.electacta.2014.12.003

[9] Yeber, M. C., Soto, C., Riveros, R., Navarrete, J., Vidal, G. "Optimization by factorial design of copper (II) and toxicity removal using a photocatalytic process with TiO_2 as semiconductor", Chemical Engineering Journal, 152(1), pp. 14–19, 2009. https://doi.org/10.1016/j.cej.2009.03.021

[10] Khulbe, K.C., Matsuura, T. "Removal of heavy metals and pollutants by membrane adsorption techniques", Applied Water Science, 8(1), 19, 2018. https://doi.org/10.1007/s13201-018-0661-6

[11] Davarnejad, R., Panahi, P. "Cu (II) removal from aqueous wastewaters by adsorption on the modified henna with Fe_3O_4 nanoparticles using response surface methodology", Separation and Purification Technology, 158, pp. 286–292, 2016. https://doi.org/10.1016/j.seppur.2015.12.018

[12] Wu, L., Wan, W., Shang, Z., Gao, X., Kobayashi, N., Luo, G., Li, Z. "Surface modification of phosphoric acid activated carbon by using non-thermal plasma for enhancement of Cu(II) adsorption from aqueous solutions", Separation and Purification Technology, 197, pp. 156–169, 2018 https://doi.org/10.1016/j.seppur.2018.01.007

[13] Ali, R. M., Hamad, H. A., Hussein, M. M., Malash, G. F. "Potential of using green adsorbent of heavy metal removal from aqueous solutions: Adsorption kinetics, isotherm, thermodynamic, mechanism and economic analysis", Ecological Engineering, 91, pp. 317–332, 2016. https://doi.org/10.1016/j.ecoleng.2016.03.015

[14] Upadhyay, R., Pandey, P. K., Pardeep "Adsorption of Cu(II) and Cr(VI) by zeolite in batch and column mode", Materials Today: Proceedings, 4(9), pp. 10504–10508, 2017. https://doi.org/10.1016/j.matpr.2017.06.409

[15] Ulucan-Altuntas, K., Uzun, H. I., Ustundag, C. B., Debik, E. "Adsorption of copper ion from aqueous solutions by well-crystalized nanosized hydroxyapatite", Materials Research Express, 6(12), 125545, 2019. https://doi.org/10.1088/2053-1591/ab66a1

[16] Danesh, N., Ghorbani, M., Marjani, A. "Separation of copper ions by nanocomposites using adsorption process", Scientific Reports, 11(1), 1676, 2021. https://doi.org/10.1038/s41598-020-80914-w

[17] Lucaci, A. R., Bulgariu, D., Bulgariu, L. "In Situ Functionalization of Iron Oxide Particles with Alginate: A Promising Biosorbent for Retention of Metal Ions", Polymers, 13(20), 3554, 2021. https://doi.org/10.3390/polym13203554

[18] Chao, H. P., Chang, C. C. "Adsorption of copper(II), cadmium(II), nickel(II) and lead(II) from aqueous solution using biosorbents", Adsorption, 18(5), pp. 395–401, 2012. https://doi.org/10.1007/s10450-012-9418-y

[19] Ibrahim, H. S., Ammar, N. S., Soylak, M., Ibrahim, M. "Removal of Cd(II) and Pb(II) from aqueous solution using dried water hyacinth as a biosorbent", Spectrochimica Acta Part A: Molecular and Biomolecular Spectroscopy, 96, pp. 413–420, 2012. https://doi.org/10.1016/j.saa.2012.05.039

[20] Murithi, G., Onindo, C. O., Wambu, E. W., Muthakia, G. K. "Removal of Cadmium(II) Ions from water by adsorption using water hyacinth (*Eichhornia crassipes*) biomass", BioResources, 9(2), pp. 3613–3631, 2014. https://doi.org/10.15376/biores.9.2.3613-3631

[21] Sarkar, M., Rahman, A. K. M. L., Bhoumik, N. C. "Remediation of chromium and copper on water hyacinth (*E. crassipes*) shoot powder", Water Resources and Industry, 17, pp. 1–6, 2017. https://doi.org/10.1016/j.wri.2016.12.003

[22] Jahangiri, F. M., Moutushi, H. T., Moniruzzaman, M., Hoque, S., Hossain, M. E. "Removal of lead from aqueous solutions and wastewaters using water hyacinth (*Eichhornia crassipes*) roots", Water Practice & Technology, 16(2), pp. 404–419, 2021. https://doi.org/10.2166/wpt.2021.005

[23] Carnerio, M. T., Barros, A. Z., Morais, A. I. S., Melo, A. L. F. C., Bezzera, R. D. S., Osajima, J. A., Silva-Filho, E. C. "Application of water hyacinth biomass (*Eichhornia crassipes*) as an adsorbent for methylene blue dye from aqueous medium: Kinetic and isothermal study", Polymers, 14(13), 2732, 2022. https://doi.org/10.3390/polym14132732

[24] Hazarika, L., Shah, K. K., Baruah, G., Bharali, R. K. "Kinetic and equilibrium studies on bioadsorption of copper and lead by water hyacinth (*Eichhornia crassipes*) plant powder", Vietnam Journal of Chemistry, 61(2), pp. 238–252, 2023. https://doi.org/10.1002/vjch.202200138

[25] Rosidah, R., Rahayu, S. Y. S., Susanti, E. "Removal of Cadmium (II) by Adsorption using Water Hyacinth (*Eichhornia crassipes*) Dried Biomass", Journal of Ecological Engineering, 24(3), pp. 246–253, 2023. https://doi.org/10.12911/22998993/156692

[26] Singh, A., Bishnoi, N. R. "Comparative study of various pretreatment techniques for ethanol production from water hyacinth", Industrial Crops and Products, 44, pp. 283–289, 2013. https://doi.org/10.1016/j.indcrop.2012.11.026

[27] Datta, R. "Acidogenic fermentation of lignocellulose–acid yield and conversion of components", Biotechnology and Bioengineering, 23(9), pp. 2167–2170, 1981.
https://doi.org/10.1002/bit.260230921

[28] Joseph, I. V., Tosheva, L., Doyle, A. M. "Simultaneous removal of Cd(II), Co(II), Cu(II), Pb(II), and Zn(II) ions from aqueous solutions via adsorption on FAU-type zeolites prepared from coal fly ash", Journal of Environmental Chemical Engineering, 8(4), 103895, 2020.
https://doi.org/10.1016/j.jece.2020.103895

[29] Qu, Y., Zhang, C., Li, F., Bo, X., Liu, G., Zhou, Q. "Equilibrium and kinetics study on the adsorption of perfluorooctanoic acid from aqueous solution onto powdered activated carbon", Journal of Hazardous Materials, 169(1–3), pp. 146–152, 2009.
https://doi.org/10.1016/j.jhazmat.2009.03.063

[30] Kalam, S., Abu-Khamsin, S. A., Kamal, M. S., Patil, S. "Surfactant Adsorption Isotherms: A Review", ACS Omega, 6(48), pp. 32342–32348, 2021.
https://doi.org/10.1021/acsomega.1c04661

[31] Oriez, V., Peydecastaing, J., Pontalier, P.-Y. "Lignocellulosic biomass mild alkaline fractionation and resulting extract purification processes: Conditions, yields, and purities", Clean Technologies, 2(1), pp. 91–115, 2020.
https://doi.org/10.3390/cleantechnol2010007

[32] Quintero, J. A., Rincón, L. E., Cardona, C. A. "Production of bioethanol from agroindustrial residues as feedstocks", In: Pandey, A., Larroche, C., Ricke, S. C., Dussap, C.-G., Gnansounou, E. (eds.) Biofuels, Academic Press, 2011, pp. 251–285. ISBN 978-0-12-385099-7
https://doi.org/10.1016/B978-0-12-385099-7.00011-5

[33] Berlin, A., Balakshin, M. "Industrial lignins: Analysis, properties, and applications", In: Gupta, V. K., Tuohy, M. G., Kubicek, C. P., Saddler, J., Xu, F. (eds.) Bioenergy Research: Advances and Applications, Elsevier, 2014, pp. 315–336. ISBN 978-0-444-59561-4
https://doi.org/10.1016/B978-0-444-59561-4.00018-8

[34] Buranov, A. U., Mazza, G. "Lignin in straw of herbaceous crops", Industrial Crops and Products, 28(3), pp. 237–259, 2008.
https://doi.org/10.1016/j.indcrop.2008.03.008

[35] Modenbach, A. A., Nokes, S. E. "Effects of sodium hydroxide pretreatment on structural components of biomass", Transactions of the ASABE, 57(4), pp. 1187–1198, 2014.
https://doi.org/10.13031/trans.57.10046

[36] Zheng, Q., Zhou, T., Wang, Y., Cao, X., Wu, S., Zhao, M., Wang, H., Xu, M., Zheng, B., Zheng, J., Guan, X. "Pretreatment of wheat straw leads to structural changes and improved enzymatic hydrolysis", Scientific Reports, 8(1), 1321, 2018.
https://doi.org/10.1038/s41598-018-19517-5

[37] Dubinin, M. M. "Micropore structures of charcoal adsorbents. 1. A general characterization of micro- and supermicropores in the fissure model", Bulletin of the Academy of Sciences of the USSR, Division of Chemical Science, 28(8), pp. 1560–1564, 1979.
https://doi.org/10.1007/BF00950967

[38] Javier-Astete, R., Jimenez-Davalos, J., Zolla, G. "Determination of hemicellulose, cellulose, holocellulose and lignin content using FTIR in *Calycophyllum spruceanum* (Benth.) K. Schum. and *Guazuma crinita* Lam.", PLoS ONE, 16(10), e0256559, 2021.
https://doi.org/10.1371/journal.pone.0256559

[39] Gonultas, O., Candan, Z. "Chemical characterization and FTIR spectroscopy of thermally compressed eucalyptus wood panels", Maderas: Ciencia y Tecnologia, 20(3), pp. 431–442, 2018.
https://doi.org/10.4067/S0718-221X2018005031301

[40] Rezania, S., Din, M. F. M., Taib, S. M, Mohamad, S. E., Dahalan, F. A., Kamyab, H., Darajeh, N., Ebrahimi, S. S. "Ethanol production from water hyacinth (*Eichhornia crassipes*) using various types of enhancers based on the consumable sugars", Waste and Biomass Valorization, 9(6), pp. 939–946, 2018.
https://doi.org/10.1007/s12649-017-9883-3

[41] Singh, J. K., Chaurasia, B., Dubey, A., Noguera, A. M. F., Gupta, A., Kothari, R., Upadhyaya, C. P., Kumar, A., Hashem, A., Alqarawi A. A., Abd Allah, E. F. "Biological Characterization and Instrumental Analytical Comparison of Two Biorefining Pretreatments for Water Hyacinth (*Eichhornia crassipes*) Biomass Hydrolysis", Sustainability, 13(1), 245, 2021.
https://doi.org/10.3390/su13010245

[42] Uddin, N., Islam, T., Das, S. "A Novel Biosorbent, Water-Hyacinth, Uptaking Methylene Blue from Aqueous Solution: Kinetics and Equilibrium Studies", International Journal of Chemical Engineering, 2014, 819536, 2014.
https://doi.org/10.1155/2014/819536

[43] Guyo, U., Moyo, M. "Cowpea pod (*Vigna unguiculata*) biomass as a low-cost biosorbent for removal of Pb(II) ions from aqueous solution", Environmental Monitoring and Assessment, 189(2), 47, 2017.
https://doi.org/10.1007/s10661-016-5728-y

[44] Li, Z., Teng, T. T., Alkarkhi, A. F. M., Rafatullah, M., Low, L. W. "Chemical Modification of *Imperata cylindrica* Leaf Powder for Heavy Metal Ion Adsorption", Water, Air, & Soil Pollution, 224(4), 1505, 2013.
https://doi.org/10.1007/s11270-013-1505-5

[45] Melichová, Z., Hromada, L. "Adsorption of Pb^{2+} and Cu^{2+} ions from aqueous solutions on natural bentonite", Polish Journal of Environmental Studies, 22(2), pp. 457–464, 2013.

[46] Ouyang, D., Zhuo, Y., Hu, L., Zeng, Q., Hu, Y., He, Z. "Research on the Adsorption Behavior of Heavy Metal Ions by Porous Material Prepared with Silicate Tailings", Minerals, 9(5), 291, 2019.
https://doi.org/10.3390/min9050291

[47] Shirzadeh, M., Sepehr, E., Rasouli Sadaghiani, M. H., Ahmadi, F. "Effect of pH, Initial Concentration, Background Electrolyte, and Ionic Strength on Cadmium Adsorption by TiO2 and γ-Al2O3 Nanoparticles", Pollution, 6(2), pp. 223–235, 2020.
https://doi.org/10.22059/poll.2019.286644.666

[48] Elkhaleefa, A., Ali, I. H., Brima, E. I., Shigidi, I., Elhag, A. B., Karama, B. "Evaluation of the Adsorption Efficiency on the Removal of Lead(II) Ions from Aqueous Solutions Using *Azadirachta indica* Leaves as an Adsorbent", Processes, 9(3), 559, 2021. https://doi.org/10.3390/pr9030559

[49] Di, J., Ruan, Z., Zhang, S., Dong, Y., Fu, S., Li, H., Jiang, G. "Adsorption behaviors and mechanisms of Cu^{2+}, Zn^{2+} and Pb^{2+} by magnetically modified lignite", Scientific Reports, 12(1), 1394, 2022. https://doi.org/10.1038/s41598-022-05453-y

[50] Putra, W. P., Kamari, A., Yusoff, S. N. M., Ishak, C. F., Mohamed, A., Hashim, M., Isa, I. M. "Biosorption of Cu(II), Pb(II) and Zn(II) Ions from Aqueous Solutions Using Selected Waste Materials: Adsorption and Characterisation Studies", Journal of Encapsulation and Adsorption Sciences, 4(1), pp. 25–35, 2014. https://doi.org/10.4236/jeas.2014.41004

[51] Hidayat, A. R. P., Sulistiono, D. O., Murwani, I. K., Endrawati, B. F., Fansuri, H., Zulfa, L. L., Ediati, R. "Linear and nonlinear isotherm, kinetic and thermodynamic behavior of methyl orange adsorption using modulated Al_2O_3@UiO-66 via acetic acid", Journal of Environmental Chemical Engineering, 9(6), 106675, 2021. https://doi.org/10.1016/j.jece.2021.106675

[52] López-Luna, J., Ramírez-Montes, L. E., Martinez-Vargas, S., Martinez, A. I., Mijangos-Ricardez, O. F., González-Chávez, M. C. A., Carrillo-González, R., Solís-Domínguez, F. A., Cuevas-Díaz, M.C., Vázquez-Hipólito, V. "Linear and nonlinear kinetic and isotherm adsorption models for arsenic removal by manganese ferrite nanoparticles", SN Applied Science, 1(8), 950, 2019. https://doi.org/10.1007/s42452-019-0977-3

[53] Nyamunda, B. C., Chivhanga, T., Guyo, U., Chigondo, F. "Removal of Zn (II) and Cu (II) Ions from industrial wastewaters using magnetic biochar derived from water hyacinth", Journal of Engineering, 2019, 5656983, 2019. https://doi.org/10.1155/2019/5656983

[54] Sun, Q., Yang, L. "The adsorption of basic dyes from aqueous solution on modified peat-resin particle", Water Research, 37(7), pp. 1535–1544, 2003. https://doi.org/10.1016/S0043-1354(02)00520-1

[55] Dizge, N., Aydiner, C., Demirbas, E., Kobya, M., Kara, S. "Adsorption of reactive dyes from aqueous solutions by fly ash: Kinetic and equilibrium studies", Journal of Hazardous Materials, 150(3), pp. 737–746, 2008. https://doi.org/10.1016/j.jhazmat.2007.05.027

[56] Liu, L., Luo, X. B., Ding, L., Luo, S. L. "Application of Nanotechnology in the Removal of Heavy Metal from Water", In: Luo, X., Deng, F. (eds.) Nanomaterials for the Removal of Pollutants and Resource Reutilization: Micro and Nano Technologies, Elsevier, 2019, pp. 83–147. ISBN 978-0-12-814837-2 https://doi.org/10.1016/B978-0-12-814837-2.00004-4

[57] Kariuki, Z., Kiptoo, J., Onyancha, D. "Biosorption studies of lead and copper using rogers mushroom biomass '*Lepiota hystrix*'", South African Journal of Chemical Engineering, 23, pp. 62–70, 2017. https://doi.org/10.1016/j.sajce.2017.02.001

[58] Dursun, A. Y. "A comparative study on determination of the equilibrium, kinetic and thermodynamic parameters of biosorption of copper(II) and lead(II) ions onto pretreated *Aspergillus niger*", Biochemical Engineering Journal, 28(2), pp. 187–195, 2006. https://doi.org/10.1016/j.bej.2005.11.003